Frindy, S.; Primo Arnau, AM.; Qaiss, AEK.; Bouhfid, R.; Lahcini, M.; García Gómez, H.; Bousmina, M.... (2016). Insightful understanding of the role of clay topology on the stability of biomimetic hybrid chitosan-clay thin films and CO2-dried porous aerogel microspheres. Carbohydrate Polymers. 146:353-361. doi:10.1016/j.cabpel.2016.03.022

Insightful understanding of the role of clay topology on the stability of biomimetic hybrid chitosan-clay thin films and CO_2-dried porous aerogel microspheres

Sana Frindy,[a,b,c] Ana Primo,[b] Abou el kacem Qaiss,[d] Rachid Bouhfid,[d] Mohamed Lahcini,[c] Hermenegildo Garcia,[b] Mosto Bousmina,[a] and Abdelkrim El Kadib.[a,*]

[a] Euromed Research Center, Engineering Division, Euro-Mediterranean University of Fes (UEMF), Fès-Shore, Route de Sidi Hrazem, 30070 Fès, Morocco.

[b] Instituto de Tecnología Química (CSIC-UPV) and Departamento de Química. (UPV), Av. de los Naranjos s/n, 46022 Valencia, Spain.

[c] Laboratory of Organometallic and Macromolecular Chemistry-Composites Materials, Faculty of Sciences and Technologies, Cadi Ayyad University, Avenue Abdelkrim Elkhattabi, B.P. 549,40000 Marrakech, Morocco.

[d] Moroccan Foundation for Advanced Science, Innovation and Research (MAScIR), Institute of Nanomaterials and Nanotechnology (NANOTECH), Laboratory of Polymer Processing, Rabat, Morocco.

ABSTRACT: Three natural clay-based microstructures, namely layered montmorillonite (MMT), nanotubular halloysite (HNT) and micro-fibrillar sepiolite (SP) were used for the synthesis of hybrid chitosan-clay thin films and porous aerogel microspheres. At a first glance, a decrease in the viscosity of the three gel-forming solutions was noticed as a result of breaking the mutual polymeric chains interaction by the clay microstructure. Upon casting, chitosan-clay films displayed enhanced hydrophilicity in the order CS<CS-MMT<CS-HNT<CS-SP. Irrespective to the clay microstructure, an improvement in the mechanical properties of the chitosan-clay films has been substantiated with CS-SP reaching the highest value at 5% clay loading. While clay addition provides a way to resist the shrinkage occurring for native chitosan, the enhanced hydrophilicity associated to the water content affects the efficacy of the CO_2 super-critical drying as the most hydrophilic CS-SP microspheres face the highest shrinkage, resulting in a lowest specific surface area compared to CS-HNT and CS-MMT. Chitosan-clay exhibits enhanced thermal properties with the degradation delayed in the order CS<CS-MMT<CS-HNT<CS-SP. Under acidic environment, a longevity has been substantiated for chitosan-clay compared to native chitosan, evidencing the beneficial protective effect of the clay particulates for the biopolymer. However, under hydrothermal treatment, the presence of clay was found to be detrimental to the material stability as a significant shrinkage occurs in hybrid CS-clay microspheres, which is attributed again to their increased hydrophilicity compared to the native polymeric microspheres. In this framework, a peculiar behavior was observed for CS-MMT, with the microspheres standing both against contraction during CO_2 gel drying and under hydrothermal conditions. The knowledge gained from this rational design will constitute a guideline toward the preparation of ultra-stable, practically-optimized food-packaging films and commercially scalable porous bio-based adsorbents.

KEY WORDS: chitosan, montmorillonite, halloysite, sepiolite, thin films, porous microspheres, super-critical drying, stability.

1. Introduction

Natural inorganic clays have become the flagship of the nanocomposite manufacturing due to several factors including their renewable nature, wide availability, relatively low cost, easy surface functionalization, high aspect ratio and low density of the clay nanosheets. The addition of low amount (~ 2-6wt%) of clay to polymeric matrices have been shown to enhance thermal and UV resistance, low permeability towards gazes and to some extent improved mechanical properties.[1,2]

The majority of the clay-polymer nanocomposite pairs concern synthetic polymer matrices,[3,4] with a quite recently increasing interest in biopolymer-clay association to design novel nano-bio-composites.[5] One of the most exciting renewable polymers in this category is chitosan; an aminopyranosic macromolecule obtained by deacetylation of natural chitin.[6] Chitin, a polysaccharide extracted from the shells of crustaceans and the exoskeletons of arthropods, is the second most abundant polymer, after cellulose, with an annual production estimated to be several billion tones.[6] Beyond the biodegradability and biocompatibility, which are common to a large spectrum of biopolymers, the ubiquitous and versatile use of chitosan is primarily attributed to the presence of transformable amino-groups on the polymer backbone. This affords quite unlimited possibilities for chitosan chemical modification and an easy-tailoring of its reactive surface-chemistry.[7] Besides, the film-forming ability of chitosan and its moldable character to shape the polymeric body as thin films, hierarchical monoliths, porous microspheres and ultrafine particles offer additional possibilities for tailoring the materials texture.[8] Probably, the most exciting and promising properties of chitosan itself lies in its capacity to afford, by sample

pH-inversion, highly porous, dispersed nano-fibrillar hydrogels.[8b, 9, 10] Chitosan-based porous hydrogels are obtained in a very simple manner, by introducing soluble chitosan acidic solution in a base bath. This fast and spontaneous pH inversion impacts directly the chemical environment of the polymeric backbone and influences the mutual interactions engaged between its own chains and solvated water molecules. Indeed, following this pH switch, soluble ammoniums belonging to chitosan are converted to insoluble amines. If the initial solution is introduced as single droplets, the fast deprotonation induces an instantaneous escape of the aminopyranose units from the water medium. Consequently, the entanglement of the network in a 3-D results in a randomly distributed polymeric chains shaped as stable, self-standing microspheres.[8b, 9, 11] Remarkably, these millimetric beads are built from a tiny amount of the polysaccharide (2 to 3%), highly dispersed as nanometric scaffold in a nearly 98% *per* mass aqueous medium. As solid porous materials derived from natural bio-resources are highly desirable, efforts were also focused on how to tune the porosity in these soft-materials.[8b, 11] Evaporative drying failed to maintain the open porous network of these hydrogels because of the capillary forces exerted on the material framework during the water removal. In contrast, supercritical drying circumvents this barrier and allows suppression of the capillary forces as no meniscus exists above the supercritical point.[8b, 11, 12] Consequently, CO_2-supercritical drying stands as an efficient method to draw these soft-hydrogels to the realm of porous, lightweight solid aerogels. These scaffolds can be used in a variety of applications in which soft-chemistry is privileged, including drug-delivery vectors, bio-sorbents and bio-engineered tissues. Due to the above-mentioned characteristics, chitosan has found applications in biotechnology, catalysis and materials science.[13,14]

In a complementary fashion, natural nacre, a brick-and-mortar material built from chitin and mineral aragonite, has constituted an idealistic bio-inspiration pathway toward well-structured, mechanically-improved bio-based materials.[15] Following this, chitosan has been paired with a number of charges including carbon-based,[16] hybrid-based[11] and inorganic-based nanometric substructures.[17] Although many "chitosan-clay" hybrids were previously reported,[18] no special focus on the role played by the clay topology during the preparation of either chitosan-clay thin films or porous microspheres has been hitherto disclosed.[19] For this, three inorganic clay substructures having different topologies, namely layered montmorillonite, nanotubular halloysite and micro-fibrillar sepiolite have been selected for pairing with chitosan biopolymer. Montmorillonite with its layered lamellar structure can induces intercalation or exfoliation depending on the polymer interaction degree.[20] Halloysite nanotubes feature different composition in their interne and outer-surface, thereby offering exciting possibilities to design amphiphilic catalytic reactors and tunable drug transporters.[21] Sepiolite topology displays excellent needle-like network with high silanol density that has proven its efficiency in adsorption and host-guest interaction.[22] In this contribution, we aimed at understanding the effect of the selected topology (lamellar, tubular or fibrillar) on the gel-forming solution, the resulting solid thin films and the CO_2-dried porous aerogel microspheres.

2. Experimental

General Remarks. Commercially available reagents and solvents were purchased from Across and Aldrich and used without further purification. Chitosan of medium molecular weight (viscosity: 200 - 800 cps and a deacetylation degree of ~ 80%) was purchased from Sigma Aldrich (CAS number: 9012-76-4). Natural montmorillonite was purchased from Southern Clay

Product Inc. (Gonzales, Texas) under the trade name of Cloisite-Na^+. It is referred to as here MMT. It was received as fine particle powder (with a cationic exchange capacity *CEC* = 95 mequiv./100 g and an interlayer spacing d_{001} = 1.2 nm. Sepiolite, referred to as here SP, was purchased from TOLSA. Its degree of purity is superior to 85% and is built from slightly aggregated fibers with length of few micrometers. Halloysite nanotubes, referred herein as HNT, with the following parameters was made available by Dragonites company (Length: 0.2-2 μm, Outside Diameter 50-70 nm, Inside Diameter 15-45 nm). Dispersions were prepared by sonication (bioblock scientific –vibra cell 75115). Optical microscopy is used for a preliminary visualization of the chitosan-clay suspension. Before observation, each suspension is prepared by sonicating the mixture for 10 minutes. Scanning electron microscopy (SEM) images were acquired by using a JEOL JSM 6300 apparatus. Diffuse reflectance infrared Fourier transform (DRIFT) spectra were monitored using NICOLET iS10 spectrometer. BET analyses were carried out using micrometric ASP2420 instrument. X-ray diffraction (XRD) patterns were obtained by using a Philips X'Pert MPD diffractometer equipped with a PW3050 goniometer (CuK_α radiation, graphite monochromator), provided with a variable divergence slit and working in the fixed irradiated area mode. Viscosities of chitosan solution and chitosan-clay solution were measured at room temperature out using the tensile machine (INSTRON) in compression mode equipped with syringe to simulate a capillary rheometer, the Poiseuille equation (1) has been used to determine the viscosity.

$$\left.\begin{aligned} \Delta P &= \frac{8\eta L}{\pi r^4} D \\ \Delta P &= \frac{F}{S} \\ D &= V S \end{aligned}\right\} \rightarrow \eta = \frac{\pi F r^4}{8 S^2 V L} \qquad (1)$$

Where η, F, r, S, L and V are the viscosity, load (extracted from the machine), needle radius, syringe section, needle length and set compression rate, respectively. Three measurements for each sample were performed and the average data of viscosity were used. The tensiometer (Dataphysics, Germany) has been used to determine the surface tension and the density for each solution using wilhelmy plate and cylindrical probe, respectively. Contact angles tests were recorded using a dynamic contact angle meter (Dataphysics, Germany) equipped with a charge-coupled-device camera and using an image capture program employing scat software. Contact angles were measured by defining a circle around the drop and recording the tangent angle formed at the substrate surface. The scat program measured this angle on the left and right sides of the snapshot and then averaged them for a final value of contact angle. The chosen liquid is water. Mechanical testing of chitosan films and chitosan-clay films were performed on an RSA G2 rheometer equipped with tensile films fixture to evaluate the dynamic mechanical properties (DMA). All films were cut in rectangular (50*5 mm^2) and the thickness of each sample was measured at three different locations and the averaged value was used. Thermogravimetric analyses (TGA) were performed on a Q500 (TA instrument) using a heating rate of 20°C/min from room temperature to 800 °C under air.

General procedure for the preparation of chitosan-clay films. Chitosan solution was prepared by dissolving 1g of chitosan in 100 mL of 1% (v/v) acetic acid solution (excess of acetic acid to completely dissolve the polymer) and stirred for 3 hours to obtain homogenous mixture. The various clay particulates (MMT, SP or HNTs) were swelled in distilled water and sonicated for 30 min (29 kHz, 150 W). The clay suspension was then added to the chitosan solution with clay contents of (2 wt%, 5 wt%, 10 wt% and 20 wt%), followed by stirring at ambient temperature for 2 hours. Chitosan-clay solutions were subsequently poured into a plastic petridish and dried

under room temperature to form thin films. For comparison, pure chitosan films were also prepared in the same way, but without addition of clay.

General procedure for the preparation of chitosan-clay microspheres. The typical procedure for preparing chitosan-clay microspheres is described below. Aqueous solution of chitosan was obtained by dissolving 1g of chitosan in 100 mL of 1% (v/v) acetic acid solution. Total dissolution was obtained by stirring for 3 hours at room temperature. Then, the clay suspension was added to chitosan gel with various amounts of clay (2 wt%, 5 wt%, 10 wt% and 20 wt%) followed by stirring at room temperature for 2 hours to obtain homogenous chitosan-clay suspension. This solution was added dropwise through a 0.8 mm syringe needle into a NaOH solution (0.1 M). The resulting chitosan microspheres were stored in the alkaline solution for 2 hours and, filtered, and washed until a neutral pH solution. The beads matured under these conditions are called "hydrogel". Alcogel microspheres were obtained by their immersion in increased solution ratio of ethanol: water (respectively: 10/90; 30/70; 50/50; 70/30; 90/10) until 100% ethanol solution. The samples were denoted as **CS**, **CS-MMT**, **CS-SP** and **CS-HNT**.

CO_2-super critical drying. Aerogel microspheres were obtained by CO_2 supercritical drying of the corresponding modified alcogels. This method consists in the extraction of the solvent above the critical point. Ethanol was replaced by liquid CO_2 and the microspheres were dried under supercritical CO_2 conditions (73.8 bar and 31.5 $^{\circ}$C) in a Polaron 3100 apparatus.

Stability under acidic conditions. 40 mg of each sample of chitosan and chitosan-clay microspheres were contacted in 3 mL of acetic acid (0.1N) solution and stirred for 1h at room temperature. The time corresponding to the dissolution of the microspheres was evaluated.

Stability under hydrothermal treatment. 100 mg of chitosan and chitosan-clay microspheres were introduced in aqueous neutral solution (3mL) and subjected to water reflux at 100 ºC for 3 hours. After that, the beads were removed, washed copiously with acetone and dried at room temperature. The stability of the materials under hydrothermal conditions was assessed by the evaluation of the shrinkage size occurring compared to native, non-treated materials (Table 2).

3. Results and discussion

3.1. Chitosan-clay gel-forming solution

The protocol used in preparing the starting solution was kept the same for the different used clays. This proceeds by preparing separately two solutions: the first one consisted in solubilizing chitosan in an aqueous acidic solution, and the second in dispersing clay in an aqueous neutral solution. The final solution was reached by mixing the two dissimilar phases and their gentle stirring at a room temperature for a period of time. While the pure chitosan acidic solution was transparent, a turbid suspension became visible upon clay addition and a cloudy solution was formed for mixtures containing up to 20% clay (Figure 1). However, the colloidal solution was found to be stable even for several months and no phase separation occurred neither the presence of large visible aggregates nor a solid precipitate. This reflects the intimate mixing of the chitosan biopolymer and its inorganic partner, irrespective of the mineral clay substructure.

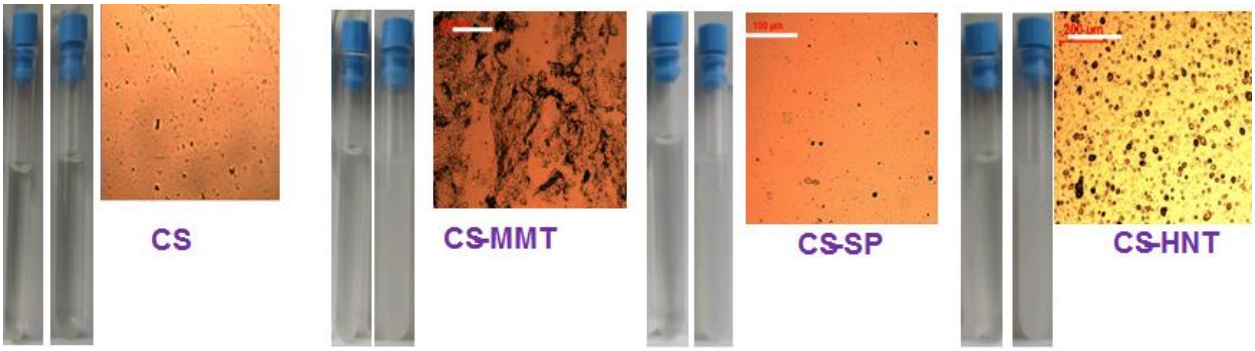

Figure 1. *Digital photos and the optical microscopic analysis of the as-prepared solutions. From left to right:* ***CS***, ***CS-MMT***, ***CS-SP*** *and* ***CS-HNT****. For CS-clay, the digital photos concern CS-clay-2% (left) and CS-clay-20% (right). The optical microscopic analysis concerns CS-clay-20%. Scale bare: 100 µm for* ***CS-MMT*** *and* ***CS-SP*** *and 200 µm for* ***CS-HNT****.*

The normalized viscosity (the ratio of the solution viscosity to that of the pure polymer) was measured and reported in Table 1. Normalized viscosity (with respect to native chitosan CS) shows at 5% loading a significant decrease in its value, being equal to 0.95 for **CS-MMT-5%**, 0.82 for **CS-SP-5%** and 0.6 for **CS-HNT-5%**. This decrease in the viscosity of the CS-clay mixture reflects the lubricating effect in accordance with the results of the previous studies.[23] In fact, the intrusion of the mineral nanoparticles between the polymer chains breaks both inter- and intra- macromolecular interactions of the network, which results in enhanced free motion of the macromolecular chains in the medium. Weaker electrostatic interaction are also suspected to take place by specific binding adsorption of the ammoniums belonging to the polymer and the hydroxyl functions (Si-OH) on the clay surface at the expense of the mutual interaction of the polymer skeleton. While hydrogen bonding between chains is known to stabilize the secondary structure of the biopolymer,[24] the interfacial adhesion is predominant during the polymer-clay interaction. Recently, molecular dynamic simulation was used to quantify chitosan and chitin

adhesion to MMT. It has been revealed that, under our similar conditions in terms of pH and deacetylation degree, chitosan binds strongly to the clay platelets, with the energy of such molecular adhesion being equal to 32.7 kcal.mol^{-1}.[12] The difference seen between **CS-SP-5%** and **CS-HNT-5%** normalized viscosities can be attributed to the size of the formed particles. Indeed, optical microscopy analysis of **CS-HNT** suspension reveals the presence of spherical particles with 15 µm in size while those observed for **CS-SP** are smaller with 9 µm in size (Figure 1 and Figure S1). More bulky are the formed aggregates, more efficient is the process of breaking chain interactions and hydrogen bonding disruption. Surprisingly, while HNT and SP possess respectively tubular and fibrillar morphology, their interplay with chitosan affords rather spherical objects which indicate that beyond wrapping the particulates, more complex multi-layer polymer-clay objects are formed in the medium. In contrast, **CS-MMT** do not afford similar spherical particulates and rather, an interconnected micro-fibrillar network is formed much probably attributed to its layered structure (Figure 1). As it will be commented later, the layered nanospace of the MMT allows the diffusion of the biopolymer inside the galleries and different scenarios can be envisioned depending on the degree of such penetration, among which one may easily distingue MMT intercalation and exfoliation. The effect of the topology on the biopolymer dynamics in solution is further illustrated by the divergent behavior observed in the surface tension upon adding MMT and HNT. While **CS-HNT-20%** increases to 53.27 mN.m^{-1} with respect to native CS solution (48.06 mN.m^{-1}), a decrease to 46.84 was noticed for **CS-MMT-20%** (Table 1).

Table 1. *Physico-chemical data of the suspension mixtures and the hybrid thin films.*

	Normalized Viscosity [a]	**Particle shape** [b]	**Particle size (µm)** [b]	**Surface Tension ($mN.m^{-1}$)** [c]	**Contact Angle (degree)** [d]	***E'* (MPa)** [e]
CS	1	-----	-----	48.06	88.5	137.02
CS-SP	0.82	spheres	9 µm	n.d	68.6	690.49
CS-HNT	0.6	spheres	15 µm	53.27	78.25	253.84
CS-MMT	0.95	Fibrils	-----	46.84	83.75	393.09

[a] *Normalized viscosity with respect to native, unmodified polymer at 5% clay loading.* [b] *Particle shape and size of the resulting chitosan-clay-20% dispersion observed by optical microscopy.* [c] *Surface tension of CS and CS-clay-20%.* [d] *Contact angle measured for CS and CS-clay-5%.* [e] *Young modulus measured for the films corresponding to CS and CS-clay-5%.*

3.2. Chitosan-clay thin film

Having revealed a slight dependency of the polymer motion to the initial topology of the used clay, we turned our attention to further evaluate their consequence on two targeted materials, thin films and porous microspheres. Thin films can be derived by an easy gelation of chitosan upon solvent evaporation. The film forms anisotropically upon drawing the biopolymer chains together to form a stacked, dense, layered network.[25]

Interestingly, whatever the amount of clay and the nature of the microstructure, high quality homogeneous bio-based films were obtained as illustrated in Figure 2 (top). The films are totally transparent with no heterogeneous zones, indicating the homogenous dispersion/distribution of

clay within the chitosan fibrils. These materials are stable, flexible and can be handled on demand.

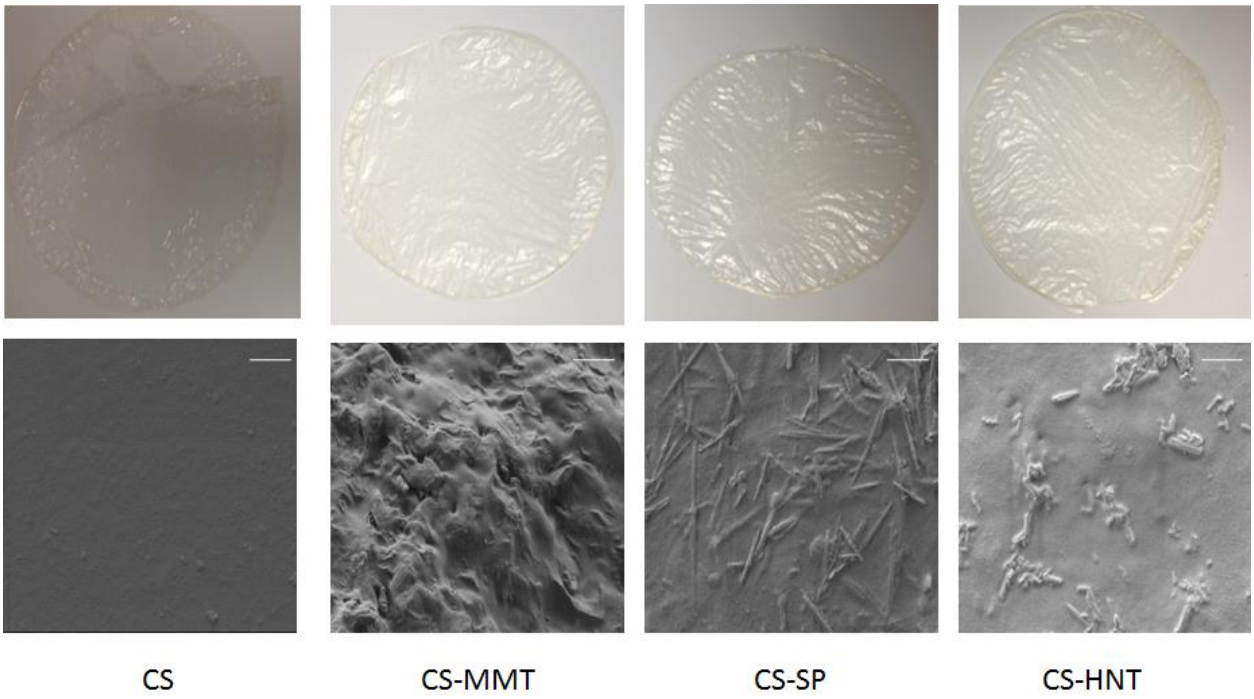

Figure 2. *Digital photos (top) and SEM analysis (bottom) of the resulting hybrid thin films. From left to right:* ***CS***, ***CS-MMT***, ***CS-SP*** *and* ***CS-HNT*** *with a clay loading of 20 wt%. (Scale bare= 1 µm).*

DRIFT analysis displays the typical pattern of chitosan biopolymer with additional peaks assignable to mineral clay phase (Figure 3 and Figure S2). The more salient evidence for polymer-clay interaction is the observation of a slight shift in the N-H deformation vibrations (δ_{NH3}) of the protonated amino groups in the pristine biopolymer (from 1580 cm^{-1} for CS to 1561, 1560 and 1558 cm^{-1} for **CS-MMT**, **CS-HNT** and **CS-SP**, respectively). This corroborates the occurrence of hydrogen bonding and electrostatic interactions between the amino and hydroxyl groups of chitosan and numerous Si-OH and Al-OH located on the surface of the various clay microstructures.[19a,23] The observation of a large band from 3000 to 3400 cm^{-1}

evidences the presence of polar OH groups as well as water molecules at the materials interface (Figure S2). This indicates that chitosan and clay are not covalently linked by means of Si-O-C bonds but interact only by hydrogen bonding.

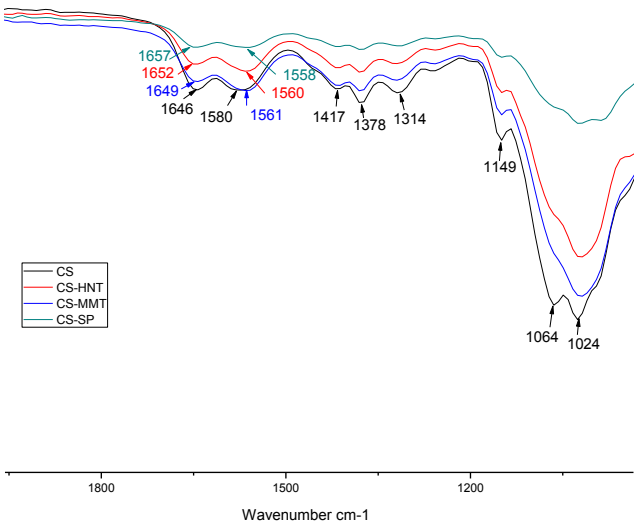

Figure 3. *DRIFT analysis of the polymeric chitosan and its hybrid CS-clay-5% version with a zoom on 1000 to 1800 cm^{-1} zone.*

Scanning electronic microscopy (SEM) allows visualization of the micrometric dispersion and distribution of the two dissimilar phases (Figure 2, bottom). Native chitosan surface is smooth probably because of the good solubility of the starting polymer at a pH ~3 value that allows total protonation of the amino groups. At a pH value of ~ 6, the less soluble polymer agglomerates and leads to more globular conformation of the chains. In such case only, chitosan deposits less uniformly, creating a rough surface.[18c] Upon clay loading, a typical rough surface is observed for **CS-MMT**, while a slightly different aspect is observed for **CS-SP** and **CS-HNT**. In fact, in these

two materials, the smooth surface is preserved, but an entanglement of the microfibrillar needle-like SP and a significant aggregation of HNT are also visible within the whole polymer. However, for all these materials, no voids, phase separation or porous network is observed, which reflects an appreciable intimate mixing of the two phases, leading to a dense stacked network during solvent evaporation.

In X-ray diffraction (XRD) analyses, typical crystalline peaks of the three mineral microstructures are visible within the as-prepared films, with no appreciable shift compared to their native structure. This confirms their intactness during the film processing (Figure 4). An additional broad peak is observed at 20° and it is unambiguously attributed to the amorphous biopolymer. In the case of **CS-HNT**, diffraction peaks at 2θ = 12°, 20° and 25° assignable to [001], [02,11] and [020] plans of raw HNT are observed. Remarkably, the intensity of the [001] reflection relative to the [02,11] band is inverted in **CS-HNT** compared to the raw clay, indicating a partial orientation of HNTs in the films during processing via interfacial interactions with chitosan. Similar behavior has been previously reported in the literature for other polymer-HNT composites.[23, 26] In **CS-SP**, the crystalline peaks of the mineral phase are preserved in the polymeric film. The intense peak at 8.5° attributed to reflections from the [110] planes in the sepiolite structure, is not shifted during chitosan adsorption. In **CS-MMT** however, a shift in the layered structure toward low angles is observed (5.5° compared to 6.9° for native sodium exchanged MMT) with the simultaneous apparition of a second crystalline peak at 2.1°. The cationic nature of protonated chitosan allows the chains to diffuse inside the galleries and ensure a cationic exchange. This intercalation expands the clay d-spacing indicated by a shift of the peak toward small angles (d = 1.47 nm and d = 4.1 n).[18a, 27]

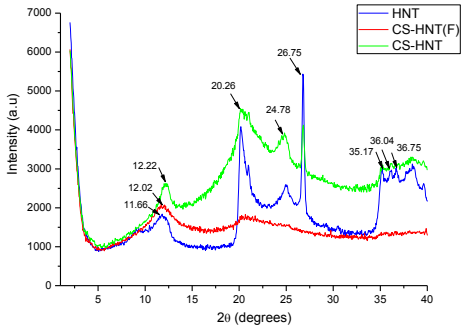

295

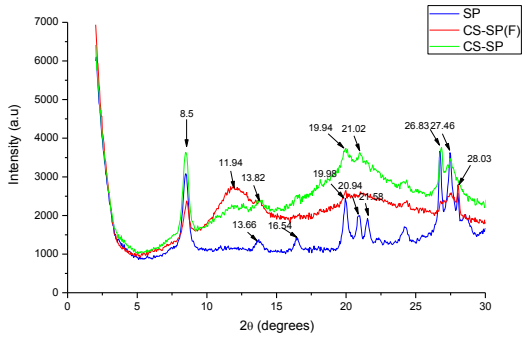

296

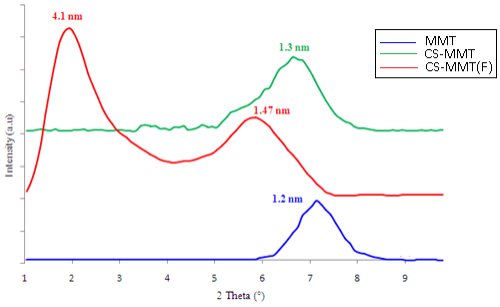

297

298 ***Figure 4****. X-ray diffraction analysis of both native clay, hybrid CS-clay thin film (CS-clay-F) and porous*
299 *CS-clay aerogel microspheres. Top:* ***CS-HNT****. Middle:* ***CS-SP****. Bottom: CS-MMT.*

300 Polysaccharides in general are known to be highly hydrophilic, with their water storage capacity
301 being the most important mechanism for plants survey and at the basis of their main application,
302 in which about 45.000 tons per year of seaweed-extracted polysaccharides are used as thickening
303 agents in the food industry.[10] The addition of 5% weight of either MMT, HNT or SP further

304 increases the hydrophilic character of the resulting hybrid films. This was evidenced by the
305 significant decrease in the contact angle of chitosan-clay films as compared to the one measured
306 for native CS films (88.5°) (Table 1). The most hydrophilic one being **CS-SP** reaching a contact
307 angle as low as 68°. This can be tentatively attributed to the abundance of Si-OH groups on the
308 sepiolite (SP) external surface while for both halloysite (HNT) and montmorillonite (MMT), a
309 large portion of polar hydroxyl groups is located inside of their confined nanopores or galleries.

310 The mechanical properties of the resulting thin films were further evaluated. In the whole, a clear
311 reinforcement effect is observed for both hybrid chitosan-clay; the Young's modulus increased
312 with the increase of the filler content. At 5% loading, the highest value was found for **CS-SP**
313 reaching 690 MPa, while the native CS displays a value of 138 MPa. **CS-MMT** and **CS-HNT**
314 record respectively 393 and 253 MPa but continue to increase with 10% loading. Up to this
315 value, the modulus drops again probably because of the clay agglomeration occurring within the
316 biopolymer. This highest value in **CS-SP** can be attributed to the high elastic modulus of single
317 sepiolite crystals and their high external surface area available for interaction with the polar
318 chains of the biopolymer.[28] The efficacy of sepiolite reinforcement with respect to palygorskite
319 has been recently reported for a variety of polymer-clay hybrids including chitosan-clay,
320 alginate-clay and starch-clay and was attributed to the difference in the level of polymer-clay
321 interaction, mainly associated to the external clay surface exposed to polymer adsorption.[19] This
322 later phenomenon seems to be connected to the dispersion/distribution degree of the mixture and
323 thus to the viscosity of the initial gel-forming solution for which **CS-SP** and **CS-MMT** formed
324 smaller aggregates compared to the bulky ones generated for **CS-HNT**. Related to this, a new
325 innovative field aiming to take benefit from different topological substructures, using both
326 layered and fibrous structure, is on the rise. One might reasonably expect an increase in the

properties of ternary composite systems featuring both 1-D and 2-D mineral (sepiolite and montmorillonite) or carbon-based (CNT and graphene) and their hybrid nanostructures.[29]

3.3 Porous chitosan-clay aerogel

As stated above, one of the objectives in the present work was to answer the following questions: i) how the initially formed chitosan-clay solution responds to the pH exchange? and if the presence of clay microstructures within the initial solution can hinder or rather favor the formation of the microspheres? In case where hydrogels can be formed, ii) how the clay microstructures affect the drying process, including the portion of the shrinkage occurring and the generated opening porosity-type (micro-, meso- and macroporosity)?

With this aim, the above-mentioned chitosan-clay solutions were added to a NaOH base bath. Whatever the clay used, all these combinations resulted in homogeneous, spherically shaped, self-standing beads. Hydrogels were then converted to alcogels by immersion in ethanol before CO_2 exchange and super-critical drying. This affords dried porous aerogel microspheres. Figure 5 and Figure S3 illustrate this multistep synthesis and clearly show a slight, marginal shrinking in the microspheres volume as the process progresses. The shrinkage percentage is provided for the two successive steps, either during hydrogel-to-alcogel and alcogel-to-aerogel transition (Table 2). The highest shrinkage in size occurs for native CS because of its well-established vulnerable nature, reaching 29% for both transitions. The results show also that independently of the clay microstructure, the shrinkage seems to be reduced compared to native CS. The maximum of the shrinkage occurs for the most hydrophilic **CS-SP** mixture, reaching 10% during hydrogel-to-alcogel transition and 23% during CO_2 gel drying. The most resistive material against shrinkage

in this series is **CS-MMT** where a marginal 4% occurs for the hydrogel-to-alcogel transition and 12% only during CO_2 drying.

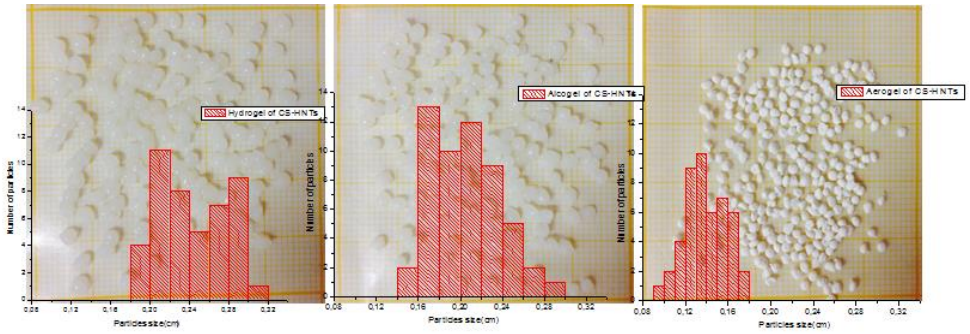

Figure 5*. Illustration of the multistep synthesis of* ***CS-HNT*** *porous microspheres from hydrogels (left), to alcogels (middle) to CO_2-dried aerogels (right). In each photo, the histogram of the average size is presented.*

It has been evidenced that core-shell microspheres built from chitosan-silica combination display a shrinkage-resistive behavior if the shell is built only from silica layers as a rigid layer influences the efficacy of the drying process.[30] The absence in these CS-clay of such a full-resistivity against contraction above the CO_2 critical point is attributed to the homogeneous distribution of the clay platelets within the microspheres, with native chitosan being on the peripheries of the beads.

Table 2. Textural parameters of the resulting porous CS and CS-clay-20% microspheres.

	Shrinkage size (%)[a]	**Shrinkage size (%)[b]**	**S_{BET}[c]**	**TGA (%)[d]**	**Dissolution time (min)[e]**	**Shrinkage size% [f]**
CS	29	29	285	60%	15	24.5
CS-SP	10	23	127	30%	30	67.6
CS-HNT	19	21	232	40%	25	51.7
CS-MMT	4	12	170	53%	35	29.6

[a] Shrinkage occurring during hydrogel-to-alcogel transition. [b] Shrinkage occurring during alcogel-to-aerogel transition. [c] Specific surface areas determined from nitrogen sorption analysis. [d] Weight degradation percentage measured at 300°C. [e] Dissolution time (min) of the microspheres during their acidic treatment. [f] Shrinkage occurring under hydrothermal conditions (water, 100 °C, 3h)

Nitrogen physisorption analysis allows to estimate the accessible surface areas of these chitosan-clay aerogels (Figure S4). Interestingly, all these materials display great porosity and specific surface areas exceeding 100 $m^2.g^{-1}$ with a nitrogen profile typical of bimodal large mesopores that continue to the macroporous domain in which the porosity is defined by the space between adjacent fibrils (Figure S5).[9, 11] Compared to native chitosan CS, CS-clay materials display reduced surface areas, decreasing in the order **CS**>**CS-HNT**>**CS-MMT**>**CS-SP** (Table 2). The location of clay between the fibrils of the support might slightly restrict the porous spaces between the fibers thereby explaining the diminution of the whole specific surface area. In support to this conclusion, a dramatic decrease of the specific surface area to 60 $m^2.g^{-1}$ has been experienced form **CS-MMT-80%** where high loading of MMT was reached.[27] Similar trend is

also observed for **CS-HNT-50%** where the measured surface area has dropped to 98 $m^2.g^{-1}$. Another probable explanation of this porosity decrease can be related to the efficiency of supercritical drying itself depending on the material composition. Indeed, although inorganic clays are well-known to improve the mechanical stability of the materials framework, their hydrophilic nature constitutes an impediment for water release from the wetted pores during ethanol: water exchange. The persisting water is undesirable during CO_2 supercritical drying because of the existing liquid-air interface, the meniscus causes pore collapsing upon gel drying. Thermodynamically speaking, the supercritical extraction of the pore fluid from a wet gel prevents the network collapse that is otherwise induced by capillary forces. These ones developed during the drying process of gels are given by the relation (2):

$$P_c = 2\,\sigma \cos(\theta_c) / r_p \qquad (2)$$

where P_c is the capillary pressure, σ is the interfacial liquid/vapor surface tension, r_p is the capillary radius and θ_c is the solid/liquid contact angle.[31]

It should be noted that, in the whole, these values must be taken carefully when compared to available literature data as even for native chitosan, fluctuation in the specific surface areas measurements are common.[9, 11, 32] Precautions are also needed in evaluating the porosity of inorganic clays as depending on their origin and chemical or thermal treatment (during mineral extraction and purification), their intrinsic properties can be different. To sum up, whatever the clay microstructure used, all chitosan-clay combinations reported herein display open-framework macro-structures exceeding 120 $m^2.g^{-1}$ making them potential eco-efficient porous adsorbents. The last point to be addressed is the thermal stability of the resulting materials which may serves as a guideline for further development of thermally-resistive chitosan-clay hybrid materials.

Expectedly, a significant improvement is noticed with the addition of clay to the CS microspheres (Figure 6). The quantification of the weight loss occurring at 300°C, which is often the limit for a number of practical applications, reveals the highest stability of **CS-SP** for which only 30% of degradation has been measured at 300°C while a 60% weight loss occurred for native non modified chitosan. In practical terms, the thermal stability increases in the order **CS<CS-MMT<CS-HNT<CS-SP**. The highest stability of **CS-SP** is further illustrated by its highest 50% degradation temperature and char residues (Table S1).

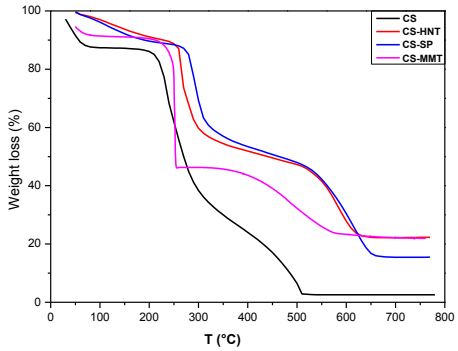

Figure 6. *Thermogravimetric degradation profile of porous CS and CS-clay-20% hybrid microspheres*

Another marked difference between thin films and porous microspheres has been substantiated by XRD measurement. In the solid CS-clay thin films, the intensity of the crystalline peaks of both SP and HNT has been significantly attenuated most probably because of the anisotropic nature of the film as well as the reorganization of the polymer framework, hindering a quantitative detection of the clay crystallinity. Deep experiments in XRD showed the sensitivity of the analyzed film to the angle of the X-ray beam and the possibility for a hidden order if the latter if perpendicular to the casting surface.[33] Once the beads are formed and the microspheres are dried, XRD reveals a substantial increase of the crystalline peaks in the microspheres compared to those initially observed in thin films (Figure 4). This can be tentatively attributed to

the reorganization of the polymer framework upon gelation where random distribution of the polymer network in the microspheres occurs accompanied by a loss of the crystallinity upon chains entanglement in the three dimensions. The amorphosition of the polymer framework allows for revealing the crystalline nature of the loaded clay substructure. In the specific case of **CS-MMT**, a spectacular behavior has been evidenced where the peak of the montmorillonite gets back to its origin (7.5°) upon pH-inversion pointing to a decrease of the interlay distance of the gallery to 1.3 nm. Indeed, deprotonation of the ammoniums located in the galleries weakened their interaction with the negatively charged montmorillonite.[12,27] The smaller Na^+ abundant in the basic NaOH solution migrates faster to the galleries and exchanges with the ammoniums. This results in immediate expulsion of the chains outside of the galleries.

3.4 Stability assessment

To assess the suitability of these eco-materials as bio-sorbents, their stability has been closely looked. Indeed, their immersion in acidic solution (0.1 N) substantially revealed the importance of clay association to hinder the polymer dissolution. While native CS dissolves within 15 minutes, the persistence of **CS-MMT** was three folds of magnitude higher reaching 45 min. This further consolidates the idea pertaining to amine occlusion by the mineral clay as chitosan dissolution is known to proceed *via* amine protonation. The highest resistivity of **CS-MMT** under acidic conditions parallels also its peculiar behavior against shrinkage during hydrogel-to-alcogel-to-aerogel passage. These two results point to an original effect assignable to the particular topology of the layered MMT as well as its interplay by intercalative mixing with the biopolymer. In comparing the stability of chitosan-titanium dioxide and chitosan-silica porous microspheres, a notable improvement for CS-TiO_2 was observed, a fact attributed to the more uniform protective layer of titanium dioxide to the polymer fibers while silica failed to reach

similar homogenous coating because of the formation of spherically aggregated silica particulates out of the fibers.[34]

Additional experiments were undertaken under hydrothermal conditions (water at 100 °C for 3 hours). In contrast to the improvement gained under acidic medium with the addition of clay particulates, the presence of these highly hydrophilic mineral phase was found to be detrimental to the material stability under boiling water treatment. This has been evidenced by the significant shrinkage occurring for CS-clay with the shrinkage percentage correlating well with the hydrophilicity of the material framework (Table 2). **CS-SP** faces the highest shrinkage (68%) under these conditions. **CS-MMT** displays again the lowest shrinkage of 29% being near to that reached for native chitosan microspheres (25%). The vulnerability seen under hydrothermal conditions can be rationalized by the hydrophilic nature of clay favoring adsorption of water molecules on the polymer framework; more hydrophilic the material is, more easy is the diffusion of water to the material framework. This high water content associated to the acidic character of clay is able to initiate a slight degradation of the glycosidic units "or at least erosion by depolymerization" of the polymer framework which may explain the highest shrinkage of the chitosan-clay microspheres under hydrothermal treatment. Indeed, while clay has found to be beneficial for improving chitosan stability under acidic conditions, their application as heterogeneous catalysts in boiling water or for the depollution of chemical stream necessitates more hydrophobic coating to be associated to the clay reinforcement.

4. Conclusion.

Herein three different clay substructure, lamellar montmorillonite (MMT), nanotubular halloysite (HNT) and micro-fibrillar sepiolite (SP) are used to design novel chitosan-clay thin films and

porous aerogels. Their high-aspect-ratio, shape, size and internal *versus* external surface were found to govern their intimate mixing with the cationic polymer. The dispersion level on the gel-forming solutions impacts the interfacial adhesion and the mechanical properties of the resulting films while the hydrophilicity depends on the intrinsic properties of the clay substructure itself. This increased hydrophilic character associated to the water content affects in turn the efficacy of the super-critical drying because of the capillary forces exerted on the material framework upon tentative removal of tightly hosted water molecules. Consequently, a significant shrinkage occurs for the most hydrophilic **CS-SP** material. Optimal clay weight loading for thin films is found to be around 5% where the maximum of the mechanical properties was reached. In turn, 20% weight loading is optimal for chitosan-clay microspheres where significant enhancement of the specific surface areas is observed and an interesting synergistic effect between the two partners is suspected. An extended chitosan-clay longevity under acidic-pH conditions was also noticed opening the way for a large scale application of these porous adsorbents in separation and pollutant removal from hostile medium. Given the specificity of each substructure, increasing performance might arise from the synergistic combination of different topologies (for instance fibrous sepiolite *versus* layered montmorillonite) and their carbon-based version (carbon nanotubes *versus* graphene) within the same biopolymer. This latter strategy may circumvent the vulnerability of the framework observed under harsh hydrothermal treatment. Work is in progress toward the preparation of ultra-stable, practically optimized food-packaging films and porous bio-based adsorbents

AUTHOR INFORMATION

Corresponding Author

Prof, Dr. Abdelkrim El Kadib: Euromed Research Center, Engineering Division, Euro-Mediterranean University of Fes (UEMF), Fès-Shore, Route de Sidi Hrazem, 30070 Fès, Morocco. a.elkadib@ueuromed.org

ACKNOWLEDGMENT.

S. F thanks MAScIR foundation, CNRST and Erasmus Mundus- Maghreb & Egypt- EMMAG.

REFERENCES

(1) Bousmina, M.; *Macromolecules*, **2006**, *39*, 4259-4263.
(2) Ray, S. S.; Okamoto, M. *Prog.Polym. Sci.*, **2003**, *28*, 1539-1641
(3) Liu, M.; Jia, Z.; Jia, D.; Zhou. Ch. *Prog. Polym. Sci*, **2014**, *39*, 1498-1525.
(4) Pavlidou, S.; Papaspyrides, C. D. *Prog. Polym. Sci*., **2008**, *33*, 1119-1198.
(5) a) Ray, S. S.; Bousmina, M. *Prog. Mater. Sci.*, **2005**, *50*, 962-1079. b) Ruiz-Hitzky, E.; Darder, M. ; Fernandes, F. M. ; Wicklein, B. ; Alcântara, A. C. S. ; Aranda. P. *Prog. Polym. Sci*, **2013**, 38, 1392-1414.
(6) a) Ferraro, V.; Cruz, I. B.; Jorge, R. F; Malcata, F. X.; Pintado, M. E.; Castro, P. M. L. *Food Research International*, **2010**, *43*, 2221-2233. b) Kojima, K.; Yoshikuni, M.; Suzuki, T. J. *Appl. Polym. Sci*. **1979**, *24*, 1587-1593.
(7) a) Rinaudo, M. *Prog. Polym. Sci*. **2006**, *31*, 603-632. b) Mourya, V. K.; Inamdar, N. N. *React. Funct. Polym*. **2008**, *68*, 1013-1051. c) Pillai, C. K. S; Paul, W.; Sharma, C. P. *Prog. Polym. Sci*. **2009**, *34*, 641-678.
(8) a) Berger, J.; Reist, M.; Mayer, J. M.; Felt, O.; Peppas, N. A.; Gurny, R. *Eur. J. Pharm. Biopharm*. **2004**, *57*, 19-34. b) El Kadib, A.; Bousmina, M.; Brunel. D. *J. Nanosci. Nanotechnol.*, **2014**, *14*, 308-331. c) Pavinatto, F. J.; Caseli, L.; Oliveira, Jr. O. N., *Biomacromolecules* **2010**, *11*, 1897 –1908.
(9) Valentin, R.; Molvinger, K.; Quignard, F; Brunel, D. *New J. Chem*. **2003**, *27*, 1690 –1692.
(10) Quignard, F.; Di Renzo, F.; Guibal, E. *Top. Curr. Chem.*, **2010**, *294*, 165-19
(11) For a review, see: El Kadib, A.; Bousmina, M. *Chem. Eur. J*. 18, **2012**, 8264-8277.
(12) Wang, Y.; Wohlert, J.; Bergenstranhle-Wohlert, M.; Tu, Y.; Agren, H.; *RSC Adv*., **2015**, *5*, 54580-54588.
(13) a) Guibal, E. *Prog. Polym. Sci*. **2005**, *30*, 71–109. b) Macquarrie, D. J.; Hardy, J. J. E. *Ind. Eng. Chem. Res*. **2005**, *44*, 8499 –8520. c) El Kadib. A. *ChemSusChem*, **2015**, *8*, 217-244.
(14) a) Jayakumar, R. ; Chennazhi, K. P. ; Muzzarelli, A. A. R. ; Tamura, H. ; Nair, S. V. ; Selvamurugan, N. *Carbohydr. Polym*. **2010**, *79*, 1–8. b) Kim, T. H.; Jiang, H. L.; Jere, D.; Park, I. K.; Cho, M. H.; Nah, J. W.; Choi, Y. Y. J.; Akaike, T.; Cho, C. S. *Prog. Polym. Sci*. **2007**, *32*, 726 –753. c) Kumar, M. N.; Muzzarelli, R. A.; Muzzarelli, C.; Sashiwa, H.; Domb, A. J. *Chem. Rev*. **2004**, *104*, 6017–6084. d) Di Martino, A.; Sittinger, M.; Risbud, M. V. *Biomaterials* **2005**, *26*, 5983–5990. e) Garcia-Gonzalez, C. A.; Alnaief, M.; Smirnova, I. *Carbohydr. Polym*. **2011**, *86*, 1425 –1438. f) Croisier, F. ; Sibret, P. ; Dupont-Gillain, C. C. ; Genet, M. J. ; Detrembleur, C. ; Jérôme, C. ; *J. Mater. Chem. B*, **2015**, *3*, 3508-3517. g) Croisier, F. ; Jérôme, C. *Euro. Polym. J.*, **2013**, *49*, 780-792.

(15) Levi-Kalisman, Y.; Falini, G.; Addadi, L.; Weiner, S. *J. Struct. Biol*. **2001**, *135*, 8-17. b) Cheng, Q.; Wu, M.; Li, M; Jiang, L.; Tang, Z. *Angew. Chem. Int. Ed*., **2013**, *52*, 3750–3755.
(16) For selected examples, see: a) Ouyang, A.; Wang, C.; Wu, S.; Shi, E.; Zhao, W.; Cao, A.; Wu, D. *ACS Appl. Mater. Interfaces*, **2015**, *7*, 14439–14445. b) Han, D.; Yan, L. *ACS Sustainable Chem. Eng*., **2014**, *2*, 296–300
(17) a) Wisser, D.; Wisser, F. M.; Raschke, S.; Klein, N.; Leistner, M.; Grothe, J.; Brunner, E.; Kaskel, S. *Angew. Chem. Int. Ed*, **2015**, *54*, 12588-12591. b) Perelshtein, IE. Ruderman, N. Perkas, T. Tzanov, J. Beddow, E. Joyce, T. J. Mason, M. Blanes, K. Molla, A. Patlolla, E.; Frenkel, A. I.; Gedanken, A. *J. Mater. Chem. B*, **2013**, *1*, 1968-1976. c) Guari, Y.; Larionova, J.; Molvinger, K.; Folch, B.; Guerin,C. *Chem. Comm*. **2006**, 2613-2615.
(18) For selected examples, see: a) Darder, M.; Colilla, M.; Ruiz-Hitzky, E. *Chem. Mater*. **2003**, *15*, 3774-3780. b) Darder, M.; Blanco, M. L.; Aranda, P.; Aznar, A. J.; Bravo, J.; Ruiz-Hitzky, E. *Chem. Mater*. **2006**, *18*, 1602-1610. c) Laufer, G.; Kirkland, C.; Cain, A. A.; Grunlan, J. C. *ACS Appl. Mater Interfaces*, **2012**, *4*, 1643-1649.
(19) By sharp contrast, more attention has been paid to the charge of the polymer, including neutral, negative and cationic matrices, see for instance: a) Alcantara, A. C. S.; Darder, M.; Aranda, P.; Ruiz-Hitzky, E. *Appl. Clay Sci*., **2014**, *96*, 2-8. b) Alcantara, A. C. S.; Darder, M.; Aranda, P.; Ayral, A.; Ruiz-Hitzky, E. *J. Appl. Polym. Sci*., **2015**, DOI: 10.1002/APP.42362.
(20) Wang, M. S.; Pinnavaia, T. J. *Chem. Mater*., **1994**, *6*, 468–474
(21) Liu, M.; Jia, Z.; Jia, D.; Zhou, C. *Prog. Polym. Sci.*, **2014**, *39*, 1498-1525. Lvov, Y.; Abdullayev, E. *Prog. Polym. Sci.*, **2013**, *38*, 1690-1719
(22) Turhan, Y.; Turan, P.; Doğan, M.; Alkan, H.; Namli, H.; Demirbaş, O. *Ind. Eng. Chem. Res*., **2008**, 47, 1883–1895
(23) Liu, M. ; Mu, C. ; Jiao,Y.; Xiong, S. ; Zhou, C. *J. Mater. Chem. B*., **2013**, *1*, 2078-2089.
(24) Harada, T.; Harada, A. In *Polysaccharide Association Structures in Food*; R. H. Walter, Ed.; Marcel Dekker: New York, **1998**; pp. 37-55
(25) Ladet, S.; David. L.; Domard, A. Nature, **2008**, *452*, 76-80.
(26) Brindley, G. W.; Robinson, K. ; MacEwan, D. M. C. *Nature*, **1946**, *157*, 225-226
(27) Ennajih, H. ; Bouhfid, R. ; Essassi, E. ; Bousmina, M. ; El Kadib, A. *Micro. Meso. Mater*., **2012**, *152*, 208-213
(28) Fernandes, F. M.; Vazquez, L.; Ruiz-Hitzky, E.; Carnicero, A.; Castro, M. *RSC Adv*., **2014**, *4*, 11225.
(29) a) Wang, J.; Cheng, Q.; Lin, L.; Jiang, L. *ACS Nano*, **2014**, *8*, 2739-2745. b) Prasad, K. E.; Das, B.; Maitra, U.; Ramamurty, U.; Rao, C. N. R. *Proc. Natl. Acad. Sci. U. S. A*., **2009**, *106*, 13186-13189. c) Shin, M. K.; Lee, B.; Kim, S. H.; Lee, J. A.; Spinks, G. M.; Gambhir, S.; Wallace, G. G.; Kozlov, M. E.; Baughman, R. H.; Kim, S. J. *Nat. Comm*., **2012**, *3*, 650.
(30) Di Renzo, F. ; Valentin, R. ; Boissière, M. ; Tourette, A. ; Sparapano, G. ; Molvinger, K. ; Devoisselle, J. M. ; Gerardin, C. ; Quignard, F. *Chem. Mater*., **2005**, *17*, 4693-4699
(31) Brinker, C. J.; Scherer, G.W.; Sol–Gel Science: The Physics and Chemistry of Sol–Gel Processing, Academic Press, San Diego, 1990.
(32) a) El Kadib, A.; Primo, A.; Molvinger, K.; Bousmina, M.; Brunel, D. *Chem. Eur. J*. **2011**, *17*, 7940 – 7946. b) El Kadib, A.; K.; Bousmina, M.; Brunel, D, *J. Catal*. **2010**, *273*, 147 –155. c) Primo. A.; Quignard, F. *Chem. Commun*. **2010**, *46*, 5593-5595. d) Frindy, S.; El Kadib, A.; Lahcini, M.; Primo, A.; Garcia, H. *ChemCatChem*, **2015**, *7*, 3307-3315. e) Frindy, S. Primo, A.; Lahcini, M. Bousmina, M. Garcia, H., El Kadib, A. *Green Chem*., **2015**, *17*, 1893-1898.

(33) Lavorgna, M. ; Piscitelli, F. ; Mangiacapra, P. ; Buonocore, G. G. *Carbohydrate Polym.*, **2010**, *82*, 291-298.
(34) a) El Kadib, A.; Molvinger, K.; Guillmon, C.; Quignard, F.; Brunel, D. *Chem. Mater*. **2008**, *20*, 2198 –2204. b) El Kadib, A.; Molvinger, K.; Cacciaguerra, T.; Bousmina, M.; Brunel, D. *Micro. Meso. Mater.* **2011**, *142*, 301-307.